Optical Engineering

OpticalEngineering.SPIEDigitalLibrary.org

Hysteresis compensation of the piezoelectric ceramic actuators–based tip/tilt mirror with a neural network method in adaptive optics

Chongchong Wang
Yukun Wang
Lifa Hu
Shaoxin Wang
Zhaoliang Cao
Quanquan Mu
Dayu Li
Chengliang Yang
Li Xuan

SPIE.

Chongchong Wang, Yukun Wang, Lifa Hu, Shaoxin Wang, Zhaoliang Cao, Quanquan Mu, Dayu Li, Chengliang Yang, Li Xuan, "Hysteresis compensation of the piezoelectric ceramic actuators–based tip/tilt mirror with a neural network method in adaptive optics," *Opt. Eng.* **55**(5), 054107 (2016), doi: 10.1117/1.OE.55.5.054107.

Optical Engineering 55(5), 054107 (May 2016)

Hysteresis compensation of the piezoelectric ceramic actuators–based tip/tilt mirror with a neural network method in adaptive optics

Chongchong Wang,[a,b] Yukun Wang,[a,*] Lifa Hu,[a] Shaoxin Wang,[a] Zhaoliang Cao,[a] Quanquan Mu,[a] Dayu Li,[a] Chengliang Yang,[a] and Li Xuan[a]
[a]Chinese Academy of Sciences, State Key Laboratory of Applied Optics, Changchun Institute of Optics, Fine Mechanics and Physics, No. 3888, Dongnanhu Road, Changchun City, Jilin Province 130033, China
[b]Chinese Academy of Sciences University, No. 19, Yuquan Road, Shijingshan District, Beijing 100039, China

Abstract. The intrinsic hysteresis nonlinearity of the piezo-actuators can severely degrade the positioning accuracy of a tip-tilt mirror (TTM) in an adaptive optics system. This paper focuses on compensating this hysteresis nonlinearity by feed-forward linearization with an inverse hysteresis model. This inverse hysteresis model is based on the classical Presiach model, and the neural network (NN) is used to describe the hysteresis loop. In order to apply it in the real-time adaptive correction, an analytical nonlinear function derived from the NN is introduced to compute the inverse hysteresis model output instead of the time-consuming NN simulation process. Experimental results show that the proposed method effectively linearized the TTM behavior with the static hysteresis nonlinearity of TTM reducing from 15.6% to 1.4%. In addition, the tip-tilt tracking experiments using the integrator with and without hysteresis compensation are conducted. The wavefront tip-tilt aberration rejection ability of the TTM control system is significantly improved with the −3 dB error rejection bandwidth increasing from 46 to 62 Hz. [DOI: 10.1117/1.OE.55.5.054107]

Keywords: adaptive optics; piezoelectric ceramic actuators; hysteresis nonlinearity; neural network.

Paper 150946 received Jul. 13, 2015; accepted for publication Apr. 27, 2016; published online May 27, 2016.

1 Introduction

Adaptive optics (AO) is a technique that measures and compensates wavefront aberrations induced by the Earth's atmosphere and by imperfections in the telescope optics to obtain the diffraction limited image.[1,2] Among these aberrations, tip/tilt (TT) disturbances are quite important. On the one hand, TT aberrations contribute more than 85% of the overall atmospheric turbulence variance.[3] On the other hand, mechanical vibrations and windshake have a significant impact on the TT aberrations, which in the case of the large telescope, are challenging to correct.[4–7] So the compensation of TT has the biggest impact on the final resolution performance of the adaptive optics system (AOS). Most AOSs use the pure integral controller for TT correction because it is simple and effective.[4] Our liquid crystal adaptive optics system tested on the 2.16 m telescope also used the integrator for the tip-tilt mirror (TTM) tracking loop.[8] Generally, for simplification, the response of TTM is assumed to be linear during the controller's design. Mostly, the integral parameter, which is tuned based on this linear system model, can guarantee the system stability and the bandwidths' requirement.[4,7] However, with the need for better TT tracking performance and higher control accuracy of the TTM in next-generation large optical telescopes, many factors need to be considered. Above all, TTM is pulled and pushed by piezoelectric ceramic actuators (PZT), which have inherent hysteresis nonlinearity. This hysteresis nonlinearity of PZT degrades the positioning accuracy of TTM and eventually reduces the TT tracking loop precision. In addition, because of the hysteresis nonlinearity, it is difficult to obtain a precise system model, which limits the system simulation and more sophisticated controller design.

In this paper, we present and validate an analytic nonlinear model to describe the complex relationship between applied voltages and the deflection of TTM with the neural network (NN). And a method for the online implementation of the inverse hysteresis model is presented, of which the computing time is at a level of microsecond. As the sampling frequency of the TT tracking loop in our AOS is about 1 kHz, this computing time can be ignored. Using this method, the static hysteresis nonlinearity of TTM reduces from 15.6% to 1.4%. Then feed-forward linearization with this inverse hysteresis model is introduced in the integrator-based TTM feedback control loop. The wavefront tip-tilt aberration rejection ability of the TTM control system is significantly improved with the −3 dB error rejection bandwidth increasing from 46 to 62 Hz. The remainder of this paper is organized as follows. In Sec. 2, the NN-based inverse hysteresis model description method is discussed. In Sec. 3, the hysteresis compensation (HC) results are given and TT tracking experiments are performed. And TT tracking performance is compared between the commonly used integrator and the integrator with the feed-forward linearization. Finally, conclusions are given in Sec. 4.

2 Theory of the Hysteresis Description Method

Many researchers have been reported to compensate the hysteresis. Kudryashov and Shmalhausen[9] compensated for hysteresis by initializing the piezo-actuator to a certain state each time before the new action, which requires extra samples and

*Address all correspondence to: Yukun Wang, E-mail: wangyukun@ciomp.ac.cn

0091-3286/2016/$25.00

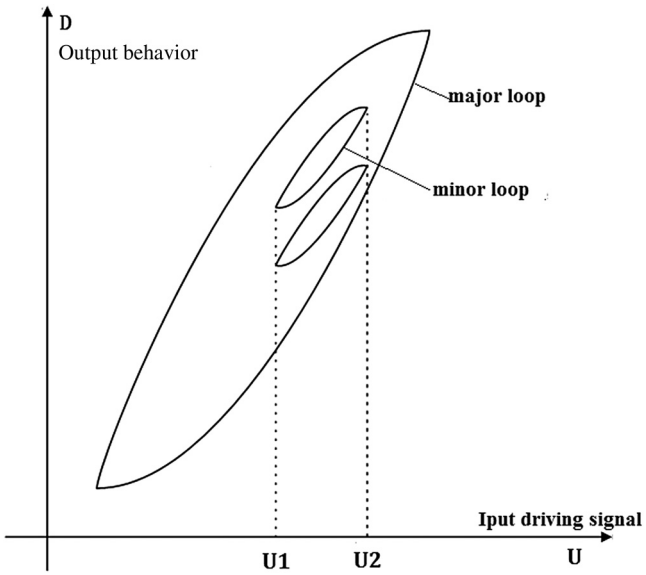

Fig. 1 Anatomy of the hysteresis loop.

thus limits the effective sampling rate of the system. Chang et al.[10] used a feedback control scheme to linearize the response of the piezo-actuator, which requires both hardware and software modification, adding to the complexity of the closed loop AO system. Another strategy was based on the hysteresis model, which compensates the hysteresis by introducing an inverse hysteresis model in the feed-forward loop of PZT. Concerning the hysteresis model structure, many methods have been used to describe the hysteresis loop branches. The scalar model of magnetic hysteresis proposed by Preisach has been used and improved by many researchers. Yang et al.[11] corrected the hysteresis of a bimorph mirror by feed-forward linearization with an enhancing Coleman–Hodgdon inverse hysteresis model. Dubra et al.[12] also reduced the hysteresis of a single-actuator bimorph mirror with a classical and a generalized Preisach inverse hysteresis model. In a word, this feed-forward linearization scheme indicates a more cost-effective approach for HC in AOS because it requires only a mathematical model instead of any hardware modification or extra samples in the control, but meanwhile provides efficient correction on hysteresis.

In the Presiach classical model, the behavior of a system with hysteresis assumes the congruency and wiping-out property.[13] Figure 1 shows the anatomy of the hysteresis loop. The congruency property states that all minor hysteresis loops with the same extreme input values are congruency. The wiping-out property means that only the alternating series of dominant input extremes are necessary to determine the current behavior of the system.

We demonstrate a simple instance to explain how the output of the inverse hysteresis model is computed. Let us consider the input–output trajectory as shown in Fig. 2. The desired displacement inputs follow $\alpha 1 \rightarrow \beta 1 \rightarrow \alpha 2 \rightarrow \beta 2 \rightarrow \alpha 3$. Here $\alpha 1$, $\alpha 2$, and $\alpha 3$ are the dominant local minima, and $\beta 1$ and $\beta 2$ are the dominant local maxima. According to the wiping-out property, the input–output trajectory following $D1 \rightarrow D2 \rightarrow D3 \rightarrow D4$ can be considered as $D1 \rightarrow D4$ directly, i.e., the local input extreme $\{\alpha 2, \beta 1\}$ can be wiped out. Define ΔV_{pq} as the voltage difference to drive TTM from position Dp to Dq, and the voltage

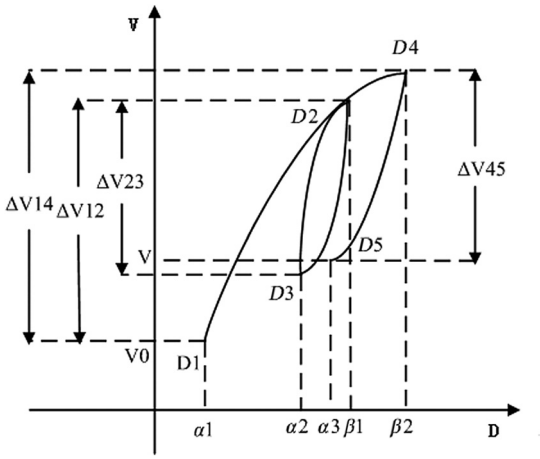

Fig. 2 Illustration of inverse Preisach model computing process.

difference ΔV_{15} that drives TTM from $D1$ to $D5$ can be computed from ΔV_{14} and ΔV_{45}. Then according to the initial voltage $V0$, the voltage needed to drive TTM from $D4$ to $D5$ is calculated as

$$V = V0 + \Delta V_{14} + \Delta V_{45}. \tag{1}$$

The congruency property indicates that hysteresis loops with the same input extremes are congruent. That means the voltage difference corresponding to the displacement extremes $\{\alpha i, \beta j\}$ is uniquely determined by these input extremes. Here we define an inverse Preisach function $P\{\alpha i, \beta j\}$ to represent the voltage difference that causes the displacement extremes $\{\alpha i, \beta j\}$. Usually, the Presiach function can be approximated by some basic functions, such as polymerization, NN. Based on MATLAB® tool, the polynomial curves of the round-trip voltage and displacement of PZT were charted by Fan Wei and Lin.[14] Though the fitting accuracy of polymerization is high, the computation of the analytic inverse function is difficult. Conclusive proofs have been given by numerous authors that multilayer neural networks are capable of approximating any continuous function to arbitrary accuracy on a compact set.[15–18] NN approximation is thus widely used in many nonlinear control systems. In this paper, a two-layer NN is used to describe the hysteresis loop branches and evaluate the inverse Preisach function. The NN consists of 10 tangent hyperbolic-neurons in the first layer and one neuron in the second layer with input (α, β) and output $P(\alpha, \beta)$ as shown in Fig. 3.

Furthermore, in order to meet the real-time computation, we use the function of back propagation NN instead of the time-consuming simulation operation to describe the hysteresis branches, which increases the computing speed and insures the computation precision as well. According to the two-layer NN structure, the $P(\alpha, \beta)$ is determined as

$$P(\alpha, \beta) = \mathrm{WL} * \tanh[\mathrm{WI} * (\alpha; \beta) + b1] + b2, \tag{2}$$

where WI and WL are the input and output weights matrix of the NN, respectively; $b1$ and $b2$ are biases on the input and output neurons, respectively. Parameters WI and WL, $b1$, and $b2$ are obtained by training the NN.

Thus, the inverse hysteresis model computation method consists of four steps: (1) train the NN with the displacement

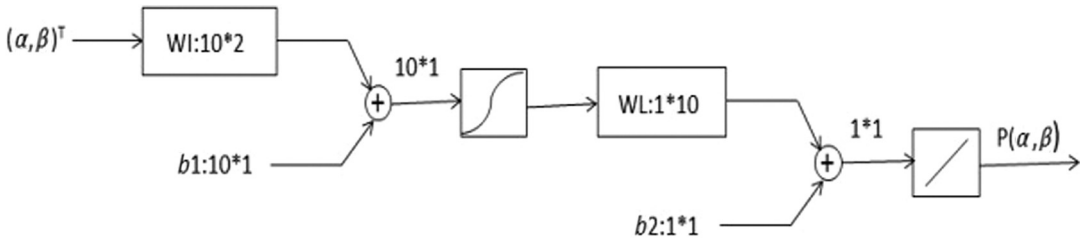

Fig. 3 Schematic representation of a two-layer NN.

and the corresponding voltage difference to get parameters of the Preisach function off-line; (2) find the displacement extremes, which determine the hysteresis loop branches on line; (3) use Eq. (2) to compute the voltage difference; and (4) use the initial voltage and voltage difference corresponding to each displacement extremes to compute the applied voltage.

3 Experiment

3.1 *Experimental Setup*

To validate the proposed HC strategy for TTM control, an experiment was conducted in the lab. Figure 4 shows the schematic of the experimental setup. The object light collimated by lens L1 was reflected by a TTM1. Then it passed through lens L2 and L3, and the wavefront TT aberrations were compensated by another TTM2. Finally, the corrected light was directed to WFS via lens L4 and L5. The TTM1 and TTM2 surface and the aperture of the WFS were conjugated with each other. In this experimental system, the two TTMs were all actuated by the PI high-dynamics piezo TT platform. TTM1 (PI S334) was used to produce the incoming TT disturbances, while TTM2 (PI S330.2SL) was used as the TT aberration corrector with a loaded resonance frequency of 2.6 kHz. By introducing TTM1, we can measure the closed-loop frequency response and error rejection frequency response of the TT control system with different control strategies. Based on the system, we can evaluate the AOS performance with and without the feed-forward HC. WFS made by our group was based on the OCAM2 camera. In the system frequency response measurement experiment, the sample rate of WFS was set to be 1 kHz on DELL T5500 work station.

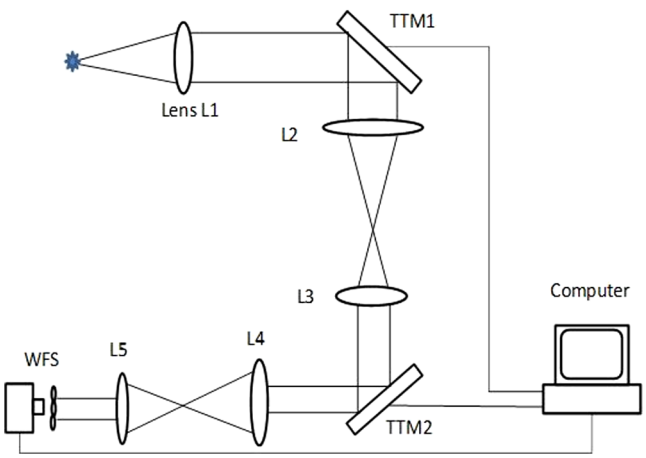

Fig. 4 Optical layout of the experimental TTM control system setup.

The block diagram of the TTM control system with feed-forward linearization is shown in Fig. 5. Φ^{tur} is the atmospheric turbulence aberrant wavefront. The TT correction signal by the TTM and the residual wavefront error are Φ^{cor} and Φ^{res}, respectively. The block TTM denotes the whole TTM control platform including high voltage amplifier, piezoelectric ceramic actuator, TT mirror, and DA convertor. $C(z)$ is a linear controller. The hysteresis compensator (HC) is introduced in the feed-forward loop to compensate the hysteresis nonlinearity and linearize the system. The static hysteresis of the PZT-based TTM with HC and without HC are measured and compared as a validation. In AOS, the higher the error rejection ability is, the smaller the residual TT is. The error rejection performance of the TTM control system is tested for tracking a sine wave with different frequencies. And the −3 dB error rejection bandwidth is used to quantitatively estimate the TT correction performance.

3.2 *Hysteresis Compensation Implementation Process*

First, we get the hysteresis data by exciting the TTM vertical axis with a sinusoidal signal denoted as $u(k)$, of which the local maxima slowly decrease in time while the local minima are kept constant. The period of the signal is 1 s to avoid exciting the system's dynamic behaviors, and the WFS sampling rate is 200 Hz. The vertical displacement (take only one axis for example) of the TTM is denoted as $y(k)$ [the pure two-sample delay caused by the detector has been removed so that $u(k)$ and $y(k)$ are already synchronized]. The input signal and hysteresis curves are shown in Figs. 6(a) and 6(b), respectively.

Based on these measured hysteresis data, the NN is trained with the extrema of displacements as the input and the corresponding voltages data set as the output. Eventually, parameters including WI, WL, $b1$, and $b2$ of the inverse Preisach function are obtained. Then, with the dominant local input displacement commands' extrema $\{\alpha i, \beta j\}$ stored and updated in real time, the desired voltage signals can be computed according to Eq. (1) and inverse Preisach function. Based on the current hardware configuration, the NN simulation process will consume more than 10 ms. The computation of inverse Presiach function takes about 5 μs, which can be ignored. Thus, the inverse hysteresis model can be used in the feed-forward loop for HC in real time.

3.3 *Simulation Results*

Figure 7(a) shows the voltages computed using the inverse hysteresis model and the actual applied voltages. The root-mean-square (RMS) of the error between the actual and the

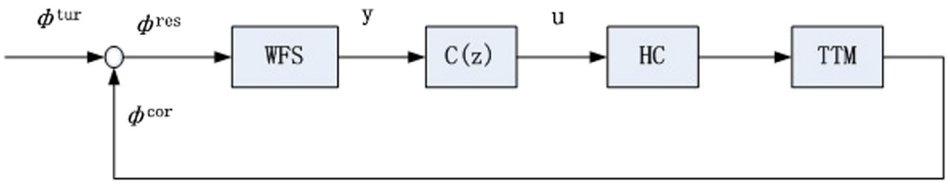

Fig. 5 Block diagram of the close-loop TTM system with an HC in the feed-forward loop.

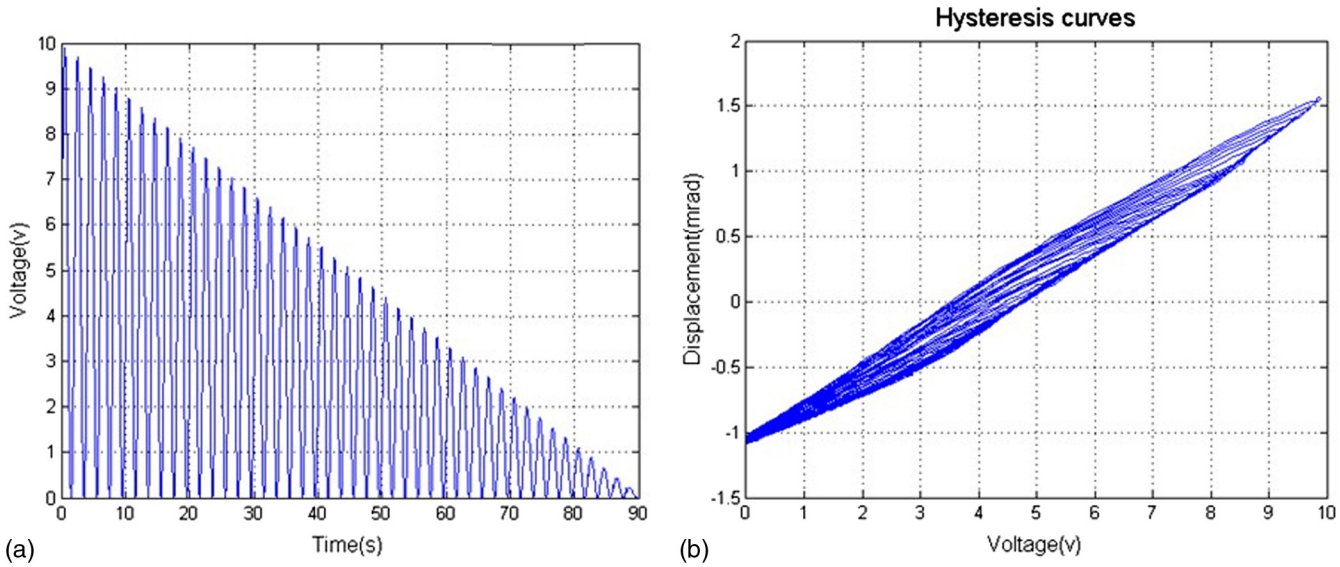

Fig. 6 Input voltage signal and hysteresis curves: (a) input voltage and (b) measured hysteresis curves.

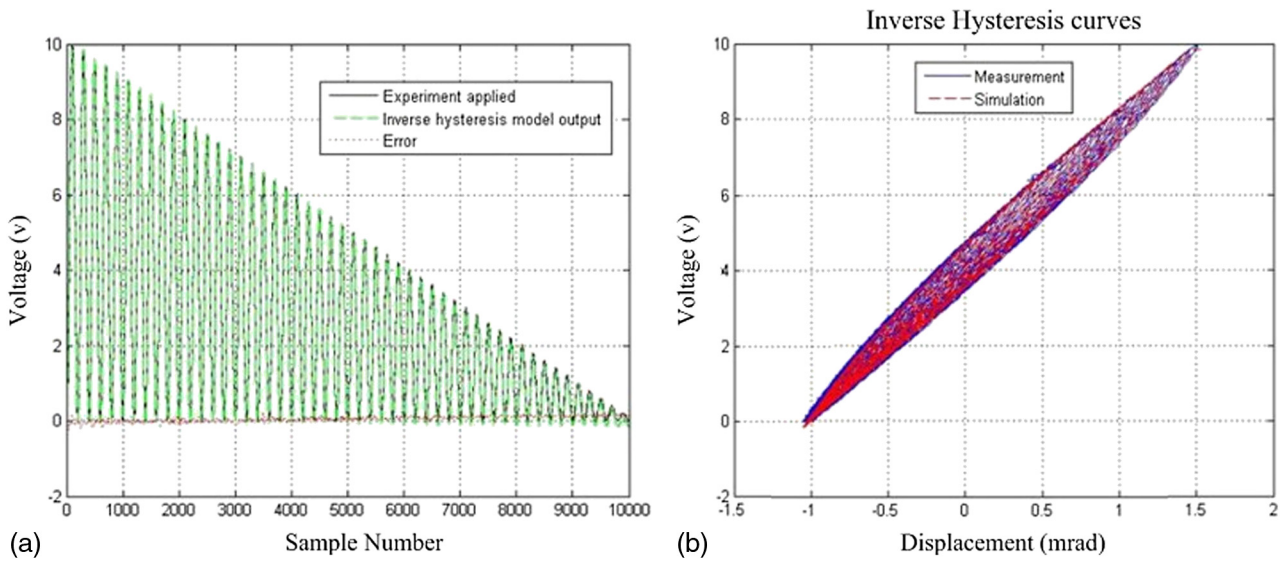

Fig. 7 The inverse hysteresis model simulation results: (a) the actual applied voltages and the inverse hysteresis model simulated output; and (b) the experimental measured and simulated inverse hysteresis curves.

inverse hysteresis model computed voltages is 0.06 V, which is only 0.6% of the voltage range. Figure 7(b) compares the measured inverse hysteresis curves in the experiment and the inverse hysteresis curves simulated using the inverse hysteresis model. The measured and simulated results agree fairly closely, which means the inverse hysteresis model can describe the TTM's inverse hysteresis property with high precision. It indicates that this model will be effective in compensating the hysteresis nonlinearity. In addition, the time used to compute the inverse hysteresis model output is tested to be at the level of a microsecond, which can be ignored in this system. Therefore, it has no effect on the open-loop dynamic property, and its transfer function can be considered as a constant.

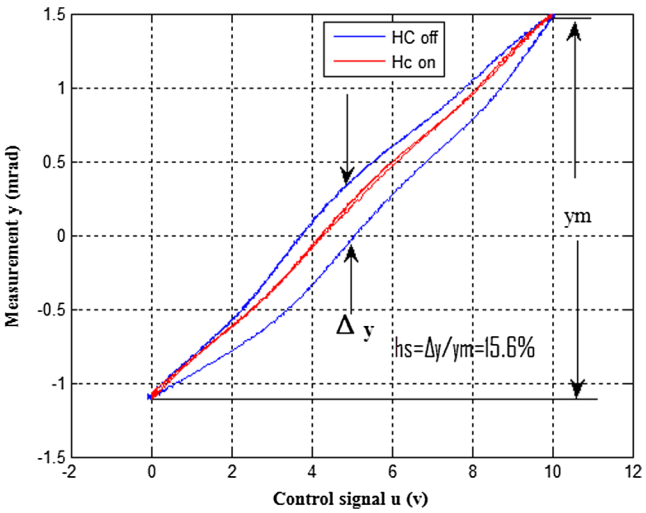

Fig. 8 The static hysteresis curves with HC on and off.

3.4 *Open-Loop Performance Comparison With and Without Hysteresis Compensation*

Experiments are conducted to test the performance of HC by exciting the vertical axis of TTM with a sinusoidal signal, of which the amplitude is 5 V with a bias of 5 V and the period is 1 s, then record the control signal $u(k)$ and vertical displacement $y(k)$ of TTM.

Figure 8 shows the hysteresis curves between the control signal $u(k)$ and the measurement $y(k)$ when HC is off and on. In order to quantify the hysteresis nonlinearity of TTM, we define hs as the ratio of the maximum possible output difference for any input (Δy) divided by the output range (ym), i.e., $hs = \Delta y/ym$ (see Fig. 8). The hysteresis parameter hs has been reduced from 15.6% to 1.4% by HC, and the linearity of the input–output curve has been improved significantly. As we can see, there still is 1.4% hysteresis nonlinearity after HC, which is mainly caused by (a) the measurement noise during the NN training; (b) the fact that the NN training input cannot cover all the excited signals in the real working condition; and (c) as discussed in Sec. 3.3, the inverse hysteresis model has error RMS 0.6%.

The open-loop TT tracking results for a reference sine signal with a frequency of 30 Hz and magnitude of 2 mrad is shown in Fig. 9. When HC is on, the open-loop tracking error RMS for the reference signal is reduced from 0.85 to 0.56 mrad. It indicates that the HC method improves the positioning accuracy of the TTM. So this method will contribute to the performance improvement of the closed-loop TTM tracking system.

3.5 *Closed-Loop Performance of Integrator With and Without Hysteresis Compensation*

To compare the TTM control system performance between the pure integral controller and the integrator with HC, closed-loop tracking experiments are conducted. In traditional controller design for the TTM, the pure integral controller's gain is adjusted based on the closed-loop step response curve. When HC is on, the system is almost linearized and the linearized system model can be identified. So we use the linearized system model and simulation to optimize the integral gain. Under the constraint of a 45 deg phase margin and a gain margin larger than 6 dB, the integral parameter is adjusted.

The result for tracking applied TT perturbation with a sine wave of 30 Hz is shown in Fig. 10. For perturbations of sine waves with different frequencies, the residual TT aberrations are listed in Table 1. The results demonstrate that when the frequency varies from 1 to 70 Hz, a higher error rejection ratio is achieved after introducing HC. Like the linear control system, with the increasing frequencies of the incoming tip signal, the error rejection ratio raises. So here we also use the bandwidth to define the error rejection ability of TTM control system quantitatively. The incorporation of a feed-forward linearization into the feedback integral control increases the −3 dB error rejection bandwidth from 46 to 62 Hz.

An experiment was also performed for tracking a data sequence of actual tip aberrations, which are obtained from the field observation with 1.23 m telescope. The tracking

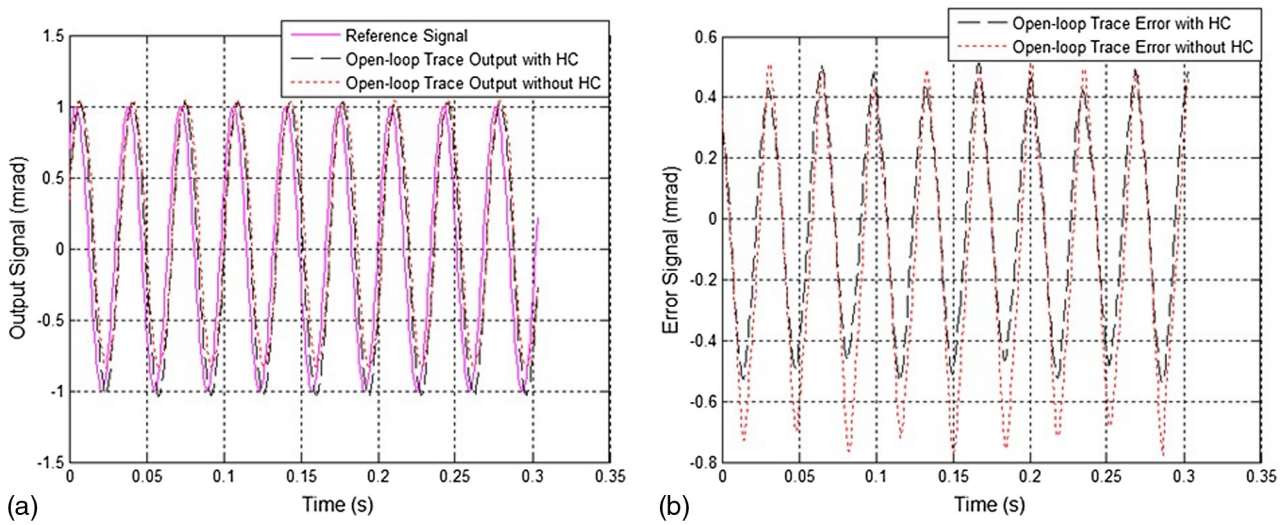

Fig. 9 Open-loop tracking results for a sine wave with frequency of 30 Hz when HC is on and off: (a) tracking output and (b) trace errors.

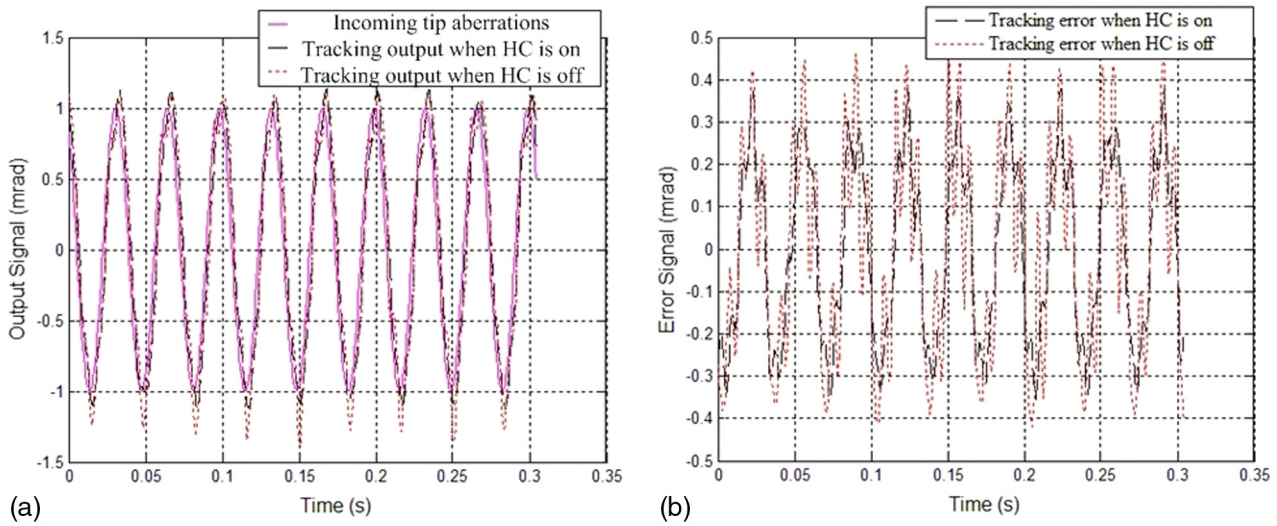

Fig. 10 Closed-loop integral control results for a sine wave frequency of 30 Hz when HC is on and off: (a) tracking output and (b) trace errors.

Table 1 Closed-loop tracking results.

Incoming TT frequency (Hz)	1	5	10	20	30	40	50	60	70
Error RMS with HC off (mrad)	0.05	0.12	0.19	0.40	0.60	0.89	1.06	1.19	1.40
Error RMS with HC on (mrad)	0.05	0.10	0.17	0.34	0.50	0.63	0.88	0.90	1.15

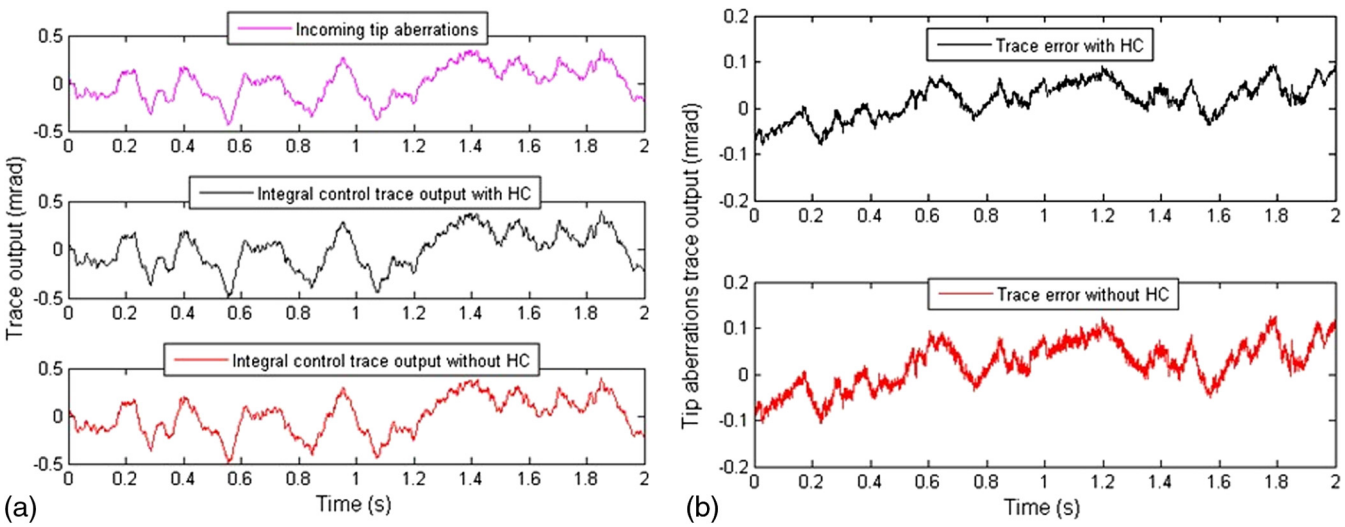

Fig. 11 Closed-loop integral control results for actual tip aberrations when HC is on and off: (a) tracking output and (b) trace errors.

results are given in Fig. 11 with (a) the vertical axis output of TTM and (b) the trace error. When HC is used with the integral control, the tracking error RMS is reduced from 0.05 to 0.038 mrad.

4 Conclusions

In this paper, we presented an inverse Preisach hysteresis model based on the function of back propagation NN instead of the time-consuming simulation operation, which increases the computing speed and ensures the computation precision as well. The comparison between the inverse hysteresis curves measured in the experiment and simulated from the inverse hysteresis models testifies to the high precision of the model in describing the inverse hysteresis property. Experimental results show that the proposed method effectively linearized the TTM behavior with the static hysteresis nonlinearity of TTM reducing from 15.6% to 1.4%. This HC method improves the positioning accuracy of the PZT without adding computation time delay to the control loop, which will improve the bandwidth of the PZT-based

tracking system. The incorporation of HC into the integral control closed-loop system has significantly improved the −3 dB error rejection bandwidth from 46 to 62 Hz. In addition, this method can be also used in many control systems with the hysteresis nonlinearity to linearize the system. The linearization of these nonlinear control systems is useful for the system simulation, controller design, and optimization and can eventually improve the control system performance.

Acknowledgments

This work was supported by the National Natural Science Foundation of China, with Grant Nos. 11174274, 61205021, 11204299, 61377032, 61378075, 61475152, and 11174279.

References

1. D. T. Gavel, "Adaptive optics control strategies for extremely large telescopes," *Proc. SPIE* **4494**, 215–220 (2002).
2. J. W. Hardy, *Adaptive Optics for Astronomical Telescopes*, Oxford University Press, Oxford (1998).
3. R. J. Noll, "Zernike polynomials and atmospheric turbulence," *JOSA* **66**(3), 207–211 (1976).
4. B. Sedghi et al., "Field stabilization (tip/tilt control) of E-ELT," *Proc. SPIE* **7733**, 773340 (2010).
5. S. Meimon et al., "Tip-tilt disturbance model identification for Kalman-based control scheme: application to XAO and ELT systems," *JOSA A* **27**(11), A122–A132 (2010).
6. C. Correia and J.-P. Véran, "Woofer-tweeter temporal correction split in atmospheric adaptive optics," *Opt. Lett.* **37**(15), 3132–3134 (2012).
7. J.-P. Véran and G. Herriot, "Woofer-tweeter tip-tilt control for NFIRAOS on TMT," *Proc. SPIE* **6272**, 62721R (2006).
8. Q. Mu et al., "Open loop adaptive optics testbed on 2.16 meter telescope with liquid crystal corrector," *Opt. Commun.* **285**(6), 896–899 (2012).
9. A. V. Kudryashov and V. I. Shmalhausen, "Semipassive bimorph flexible mirrors for atmospheric adaptive optics applications," *Opt. Eng.* **35**(11), 3064–3073 (1996).
10. M. P. J. L. Chang et al., "Hysteresis correction of a piezoelectrically actuated segmented mirror," **3353**, 864–871 (1998).
11. Q. Yang et al., "Hysteresis correction in the curvature adaptive optics system," *J. Opt. Soc. Am. A* **22**(1), 142–147 (2005).
12. A. Dubra, J. S. Massa, and C. Paterson, "Preisach classical and nonlinear modeling of hysteresis in piezoceramic deformable mirrors," *Opt. Express* **13**(22), 9062–9070 (2005).
13. A. Visintin, "Mathematical models of hysteresis," in *Modelling and Optimization of Distributed Parameter Systems Applications to Engineering*, K. Malanowski, Z. Nahorski, and M. Peszyńska, Eds., pp. 71–80, Springer, US (1996).
14. Y. X. f. Fan Wei and X. Lin, "Research on driving system and controlling means of PZT," *Opt. Precision Eng.* **15**(3), 368–371 (2007).
15. J.-C. Ban, C.-H. Chang, and S.-S. Lin, "On the structure of multi-layer cellular neural networks," *J. Differ. Equat.* **252**(8), 4563–4597 (2012).
16. C. M. Bishop, "Neural networks and their applications," *Rev. Sci. Instrum.* **65**(6), 1803–1831 (1994).
17. D. Svozil, V. Kvasnicka, and J. Pospichal, "Introduction to multi-layer feed-forward neural networks," *Chemom. Intell. Lab. Syst.* **39**, 43–62 (1997).
18. L. O. Chua, "Cellular neural networks: applications," *IEEE Trans. Ciucuits Syst.* **35**(10), 1273–1290 (1988).

Chongchong Wang received her MS degree in 2013 from the Chinese Academy of Sciences University, where she is currently pursuing her PhD. Her research interests include adaptive control and optical signal processing.

Yunkun Wang received his MS degree 2012 form the Beihang University. Now he is working in the Changchun Institute of Optics, Fine Mechanics and Physics, Chinese Academy of Sciences. His research includes control theory and system identification.

Biographies for the other authors are not available.